physica status solidi

pss

www.pss-journals.com

reprint

WILEY-VCH

Phys. Status Solidi C **11**, No. 3–4, 505–508 (2014) / **DOI** 10.1002/pssc.201300639

physica status solidi c
www.pss-c.com
current topics in solid state physics

Characterization of InGaN quantum disks in GaN nanowires

A. Roshko*, R. H. Geiss, J. B. Schlager, M. D. Brubaker, K. A. Bertness, N. A. Sanford, and T. E. Harvey

National Institute of Standards and Technology, Physical Measurement Laboratory, 325 Broadway, Boulder, Colorado 80305, USA

Received 30 September 2013, accepted 13 December 2013
Published online 4 March 2014

Keywords gallium nitride, nanowires, transmission electron microscopy, photoluminescence

* Corresponding author: e-mail roshko@boulder.nist.gov, Phone: +01 303 497 5420

Catalyst-free GaN nanowires with InGaN quantum disks (QDs) were characterized by scanning/transmission electron microscopy (S/TEM) and photoluminescence. A variety of structures, from QDs with large strain fields to apparently strain free QDs were observed. TEM lattice imaging revealed dislocations in the QD regions of the samples. Stacking faults were also observed and appear to be associated with the GaN growth temperature rather than the presence of indium. Energy dispersive X-ray spectroscopy in the TEM revealed indium concentrated in stacking faults but not always localized in the QD regions. Photoluminescence spectra show a red-shift, possibly associated with indium concentration.

© 2014 WILEY-VCH Verlag GmbH & Co. KGaA, Weinheim

1 Introduction GaN nanowires are currently of great interest due to their potential advantages over thin films for a variety of applications. Because of their high aspect ratio, nanowires can be grown on lattice mismatched substrates (including silicon) with negligible strain and low dislocation densities. Their small diameter may also reduce strain associated with lattice mismatched layers, such as InGaN quantum disks which are of interest for optical applications.

We have examined the defects and strain in nanowires grown under a variety of conditions, with InGaN quantum disks of varied thickness and composition. Dislocations were observed in the QD regions of all samples except the one with no indium and strain in the QD region was highest in the samples with the highest indium compositions. Stacking faults were found in samples with GaN grown at relatively low temperature. Photoluminescence measurements are also presented.

2 Experimental methods

2.1 Nanowire growth Catalyst-free GaN nanowires with InGaN nanodisks were grown on n-type, low-resistivity (111) silicon substrates by plasma-assisted molecular beam epitaxy (PAMBE). The substrates were cleaned in dilute HF then outgassed in the growth chamber to remove the native oxide. An AlN buffer layer was grown, after which the nanowire growth was initiated. Details of the nanowire growth have been described previously [1]. The specific conditions used for the nanowires in this study are given in Table 1. The V-III ratio was determined from the Ga and active N fluxes. The Ga flux was calibrated from low-temperature, N-rich planar film growth rate measurements, where the Ga flux is proportional to growth rate. The active N flux was quantified using the growth rate at stoichiometric fluxes (V/III = 1) and was identified by the transition between spotty and streaky reflection high energy electron diffraction (RHEED) patterns during film growth. The reported temperatures were measured by back-side-pyrometry [2]. All samples but one were grown in the same growth system.

2.2 Characterization The as grown nanowires were imaged by both field emission scanning electron microscopy (SEM) and Cs[1] probe corrected scanning/trans-mission electron microscopy (S/TEM). High resolution TEM and STEM images were taken along the [11-20] zone axis (ZA) for all samples except D062. It was not possible to tilt D062 NWs to the [11-20] ZA due to sample holder limitations. Typically 5 nanowires, with diameters from 50 to 150 nm, were examined for each sample. To enhance visibility of dislocations along both the a- and c-axes, the TEM images were analysed by inverse fast Fourier transforms (IFFT), using masks around the (0002), (10-10) and (11-20) reflections. The IFFTs were also used to determine the axial and in-plane strain adjacent the QDs. The

[1] Cs is spherical aberration.

© 2014 WILEY-VCH Verlag GmbH & Co. KGaA, Weinheim

Table 1 Growth conditions.

Samples	D134	D062	D086	D117[1]	C069[2]
Ga BEP[3] (Torr)	9.40E-9	1.30E-7	6.05E-8	6.02E-8	3.00E-8
In BEP[3] (Torr)	2.90E-8	2.25E-8	1.90E-8	0	2.00E-8
In/(In+Ga) (%)	76	15	24	0	40
N plasma (W,sccm)	300, 1	300, 1	300, 1	300, 1	350, 3
V:III ratio	8.8	0.6	1.4	1.4	not measured
T base GaN (°C)[4]	810	825	810	815	855
T InGaN QWs (°C)[4]	595	595	590, 580, 580	-	545
thickness InGaN QWs (nm)[5]	5 x 3	60, 8, 4	8, 4, 4	0	3
T GaN spacers (°C)[4]	595	825	675, 580, 580	585, 675, 585	855
thickness GaN spacers (nm)[5]	5 x 11	204, 204, 204	111, 67, 11	18, 100, 85	300

[1] Sample D117 was a repeat of D086, but with no indium. So the same temperature sequence was used.
[2] Sample C069 was grown in a different growth system then the other samples.
[3] Beam equivalent pressure.
[4] All temperatures were measured with back-side-pyrometry [2].
[5] Nominal thickness is based on growth rate measurements and is reported from the lowest to the top in the NW.

strained lattice spacing was taken to be the average of ten planes in the QD region measured from the IFFT; the unstrained lattice spacing was taken to be the average of ten planes measured in an IFFT away from the strained QD region. High angle annular dark-field (HAADF) STEM images were taken to examine the indium distribution in the samples. The detector acceptance angle for these images was 60 to 250 mrad. Energy dispersive X-ray spectroscopy (EDS) measurements were made to confirm the presence of indium in bright regions of HAADF images.

Photoluminescence (PL) measurements were performed on as-grown samples (NWs still attached to the substrate) in a front-surface geometry with excitation light from a 2 mW HeCd laser at 325 nm. The unfocused excitation beam with diameter of roughly 1 mm was incident upon the nanowire tops (c-plane), and PL was collected from the same side through a collection lens and fiber jumper. The jumper was connected to a UV-VIS CCD spectrometer, which provided the spectral data.

The spectroradiometric response of the CCD spectrometer was calibrated with a standard halogen lamp over a wavelength range of 400 to 750 nm. The spectrometer response outside this region is not calibrated, but the relative peak intensities should remain consistent from measurement to measurement.

3 Results and discussion The wurtzite nanowires grew along the [0001] axis with hexagonal cross-sections, although most are not regular hexagons. The nanowires had lengths from 1.5 to 10 µm and diameters from 50 to 300 nm. Cross-sectional SEM images of D134 and D086 (Fig. 1) show typical features. For all samples NW growth was perpendicular to the substrate. The NWs were tapered in all samples except C069, which had straight sided NWs, and the NW length was homogeneous except in sample D134. The thickness of the "matrix layer" [1] was less than 500 nm for all samples.

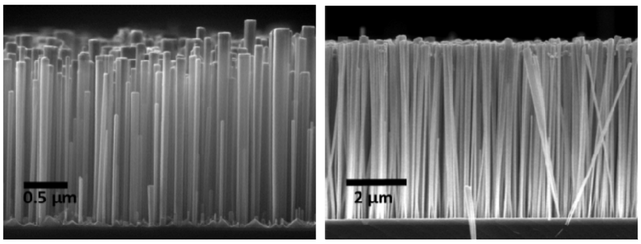

Figure 1 Cross-sectional SEM images of samples D134 and D086, showing typical growth morphologies.

TEM examination revealed that in all but one sample the wires grew with (11-20) facets. In sample D062 the side facets were (1-100). Stacking faults (SFs) in hexagonal close-packed crystals are visible along the [11-20] ZA but not along the [1-100] ZA [3]. Stacking faults were observed in the TEM images of all samples with (11-20) facets, although there were very few in C069. It was not possible to image SFs in D062 due to the (1-100) side facets.

TEM images of sample D086 (e.g. Fig. 2) show a fairly high density of stacking faults (~5 nm spacing) near the InGaN QDs. IFFTs of the (0002) and (11-10) reflections reveal dislocations in this region both parallel and perpendicular to the NW growth axis. Similarly high dislocation densities were found for samples D134 and D069. The fact that dislocations were not observed in sample D117, which

© 2014 WILEY-VCH Verlag GmbH & Co. KGaA, Weinheim

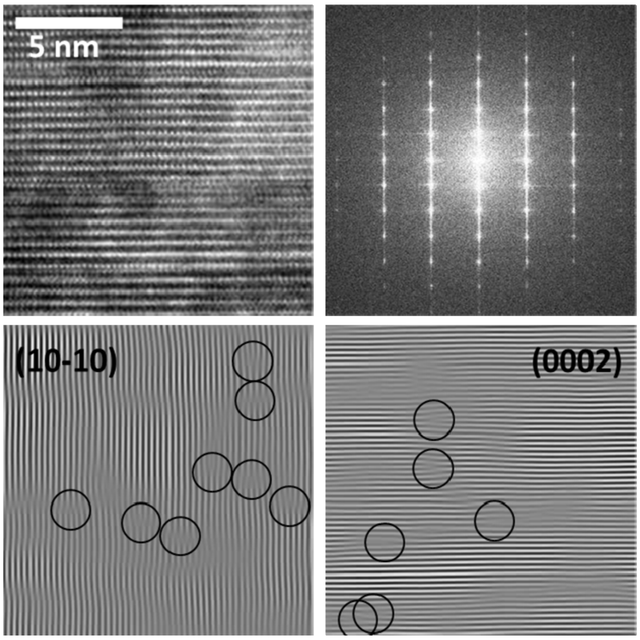

Figure 2 TEM image of D086 NW, FFT of the image and IFFTs from the (10-10) and (0002) reflections. The IFFTs show dislocations (circled) along orthogonal crystal directions.

was grown under the same conditions as D086, but with no In, suggests that the dislocations may be related to the presence of In, which is expected to expand the lattice. In D062 dislocations were found using the IFFT of the (11-20) reflection, but not with the (0002) reflection. This is consistent with minimal strain along the nanowire axis and suggests stacking faults are not present in this sample.

A summary of the defects and strain measured in the various samples is given in Table 2. The fact that there was no measureable strain in sample D062 is again consistent with a lack of stacking faults in this sample. Sample C069 also has relatively few SFs. For both of these samples a comparatively high temperature was maintained for all GaN growth (825 and 855 °C versus 585 to 675 °C for the other samples). This is consistent with previous work showing an inverse correlation between SF density and growth temperature for InGaN NWs [4].

STEM BF/HAADF images indicate that indium is concentrated along stacking faults, both in the quantum disk regions and below the quantum disks (Fig. 3). As mentioned earlier, EDS measurements confirmed the presence of indium in regions that appear bright in the HAADF image and lower levels or absence of indium in regions that are not bright. A low level of indium, not just in the quantum disk region, was found throughout sample D062. Sample D086, shown in Fig. 3, was grown with three QDs of nominal thickness 3, 3 and 7 nm, which should be located at depths of approximately 11, 80 and 200 nm, respectively. From the HAADF images it appears that the In has diffused along SFs and is not necessarily localized in the expected QD regions. The delocalized indium distribu-

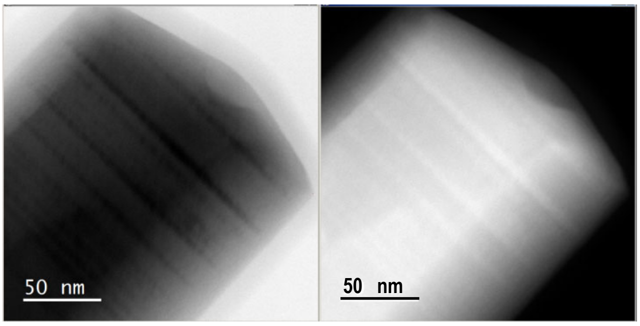

Figure 3 STEM BF and HAADF images of D086 NW with FFT of the image and IFFTs from the (10-10) and (0002) reflections.

tions in samples D062 and D086 were corroborated by atom probe tomography measurements [5].

The PL spectra for all samples exhibited a room-temperature, near-band-edge GaN peak at 363 nm (Fig. 4). Two of the samples also had weaker sub-bandgap luminescence at longer wavelengths. The sub-bandgap luminescence may in part be due to luminescence from the presence of InGaN in the nanowires. The peak sub-bandgap emission for sample D134 with a target In concentration of 76% was indeed red shifted (peak at ~ 670 nm) from that of D062 (peak at ~ 480 nm) whose target In concentration was 15%. The sub-bandgap luminescence from the other samples was weak if not absent, which was expected for the In-free sample D117 but was unexpected for samples C069 and D086, which had target In concentrations of 40% and 24% respectively.

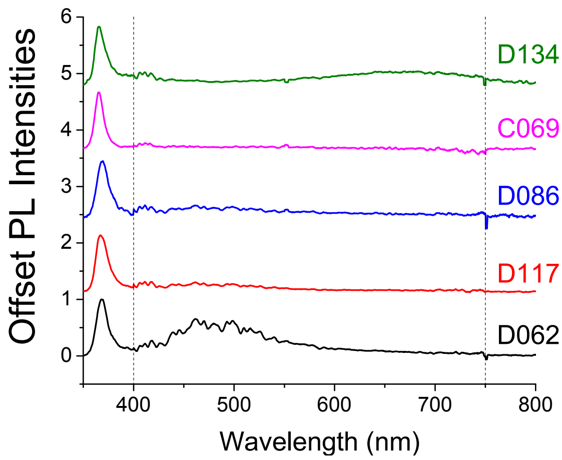

Figure 4 Photoluminescence spectra from each of the samples. The intensities have been normalized to the near-band-edge GaN peak at 363 nm. The spectrometer response between the vertical lines was calibrated and, although uncalibrated outside of this region, the relative peak intensities should be consistent from measurement to measurement (see text).

 © 2014 WILEY-VCH Verlag GmbH & Co. KGaA, Weinheim

Table 2 Defects and strain.

Samples	D134	D062[1]	D086	D117	C069
Dislocations	yes	in-plane	yes	rare	yes
Stacking Faults	yes	NV[2]	yes	yes	rare
e [0001] [3]	0.10	0	0.06	0.01	0.08
e [1-100] [3]	0.02	0[4]	0.02	0.03	0.03

[1] Imaged along [1-100] ZA.
[2] NV = not visable due to ZA.
[3] *e* is the strain measured along the designated crystal direction, $e = \Delta L/L$.
[4] Measured along [11-20].

References

[1] K. A. Bertness, A. Roshko, L. M. Mansfield, T. E. Harvey, and N. A. Sanford, J. Cryst. Growth **310**, 3154 (2008).
[2] K. A. Bertness, M. D. Brubaker, T. E. Harvey, S. M. Duff, A. W. Sanders, and N. A. Sanford, Phys. Status Solidi C **11**, 590 (2014).
[3] A. Howie, Metallurg. Rev. **6**, 467 (1961).
[4] T. Tabata, J. Paek, Y. Honda, M. Yamaguchi, and H. Amano, Jpn. J Appl. Phys. **52**, 08JE06-1 (2013).
[5] N. A. Sanford et al., Phys. Status Solidi C **11**, 608 (2014).

© 2014 WILEY-VCH Verlag GmbH & Co. KGaA, Weinheim